Light-Emitting Characteristics of Organic Light-Emitting Diodes with Ba/Al Cathode and Effect of Ba Thickness by Measuring their Built-in Potential

Jong Tae Lim and Geun Young Yeom*

School of Advanced Materials Science and Engineering, Sungkyunkwan University, Suwon 440-746, Korea

Received June 29, 2009; accepted September 14, 2009; published online December 21, 2009

The electronic nature of metal–organic semiconductor contacts is a fundamental issue in the field of organic semiconductor device physics, because these contacts control the charge injection. The built-in potential in organic light-emitting diodes (OLEDs) with a Ba/Al cathode was investigated by using the modulated photocurrent technique. To measure the built-in potential, a device with a glass/tin-doped indium oxide (ITO)/tris(8-quinolinolato)aluminum (III) (Alq_3, 150 nm)/Ba (x nm, $x = 3$, 2, 1, and 0)/Al (150 nm) structure was fabricated and encapsulated in a nitrogen atmosphere. The device with Ba/Al cathode showed a higher built-in potential, compared with the Al-only device, which reduced the barrier height for electron injection from the Ba/Al cathode to Alq_3. For the device with a Ba thickness of 3 nm, the barrier height for electron injection showed a low value of 0.1 eV. On the basis of the built-in potential data, the device with the ITO/4,4′,4″-tris(2-naphthylphenyl-1-phenylamino)triphenylamine (2-TNATA, 30 nm)/4,4′-bis(*N*-(1-napthyl)-*N*-phenyl-amino)-biphenyl (NPB, 18 nm)/Alq_3 (62 nm)/Ba (3 nm)/Al (100 nm) structure showed the best characteristics with the highest luminance of 54,000 cd/m^2 and the highest efficiency of 2.7 lm/W, as compared to the other devices with Ba thicknesses of less than 3 nm.

DOI: 10.1143/JJAP.48.122102

1. Introduction

Recently, a great deal of research interest has been focused on functional molecular organic thin films, because of their potential use in a wide variety of optoelectronic devices, such as organic light-emitting diodes (OLEDs),[1,2] organic solar cells,[3] and organic sensors.[4] Among these devices, OLEDs have continued to be developed for applications in flat-panel displays to meet the growing demand for information display units. A crucial process in the physics and operation of OLEDs is the carrier injection from the electrodes into the emitting layer. The injection probability is strongly dependent on the mismatch between the Fermi levels (E_F) of the electrodes and the relevant levels for conduction in the OLED, i.e., the injection barrier height.[5] The fact that the barrier height is typically not pinned in organic/metal contacts[6] and is thus strongly dependent on the work function of the electrode, allows its minimization by employing low work-function metals as the cathode[7] and high work-function conductors as the anode.[8] This asymmetry in their work functions also results in a large asymmetry of the barrier heights to hole and electron injection.

Moreover, in devices in which the anodic barrier is already low, since electrons typically have lower mobility than holes, a major improvement in their efficiency and lifetime can be achieved by using low work-function cathodes[9–14] such as calcium (Ca), magnesium (Mg), lithium (Li), cesium (Cs), strontium (Sr), and samarium (Sm). Recently, improved performance and stability were obtained by inserting a thin insulating film of either lithium fluoride (LiF)[15,16] or cesium fluoride (CsF)[17] between a more stable cathodic metal (such as Al) and an electron-transporting layer (ETL). These low work-function systems can significantly improve the electron injection by lowering the lowest unoccupied molecular orbital (LUMO) level.[15–17]

Meanwhile, the built-in potential (V_{BI}) can be used to determine the barrier height for electron injection across the organic layer from the cathode into the OLED. This V_{BI} in the device corresponds to the difference in the work function between the anode and the cathode. Furthermore, this built-in electric field is generated by the alignment of the Fermi level of the two electrodes in the device. The electroabsorption and modulated photocurrent techniques have frequently been used to determine the value of V_{BI} experimentally.[18–21] In 1999, Brown *et al.* reported that the V_{BI} can be increased by 0.5 V by inserting a poly(ethylene dioxythiophene)/poly(styrene sulfonic acid) (PEDOT/PSS) layer in the device.[18]

This article describes the light-out coupling properties of OLEDs, based on the work function of the Ba (x nm, $x = 3$, 2, 1, and 0 nm)/Al (150 nm) cathode. Here, Ba has a low work function of 2.7 eV.[22] Although the Ba/Al cathode system has been previously reported,[23,24] its electron injection properties have yet to be investigated in detail. To understand the electron injection characteristics from the Ba/Al cathode system into Alq_3 as a function of the Ba thickness, the barrier height (Φ_B) for electron injection in the devices was determined from V_{BI} measured by the modulated photocurrent technique.

2. Experimental Procedure

The device structure of the OLED was composed of glass/tin-doped indium oxide (ITO, about 10 Ω/square)/4,4′,4″-tris(2-naphthylphenyl-1-phenylamino)triphenylamine (2-TNATA, 30 nm)/4,4′-bis(*N*-(1-napthyl)-*N*-phenyl-amino)-biphenyl (NPB, 18 nm)/tris(8-quinolinolato)aluminum(III) (Alq_3, 62 nm)/Ba (x nm, $x = 3$, 2, 1, and 0 nm)/Al (150 nm). The Ba thicknesses in devices 1, 2, 3, and 4 were 3, 2, 1, and 0 nm, respectively. Organic layers (2-TNATA/NPB/Alq_3) consisting of 30-nm-thick 2-TNATA as a hole-injecting layer (HIL), 18-nm-thick NPB as a hole-transporting layer (HTL), and 62-nm-thick Alq_3 as both an electron injection layer (EIL) and an emissive layer were sequentially deposited by using a thermal evaporator system. A x-nm-thick Ba layer and 150-nm-thick Al layer forming a multilayer cathode (Ba/Al) were also deposited onto the multi-organic layers by using a thermal evaporator. Finally, each device was encapsulated by depositing a bead of epoxy around the edge of the substrate, sticking a piece of glass on

*E-mail address: gyyeom@skku.edu

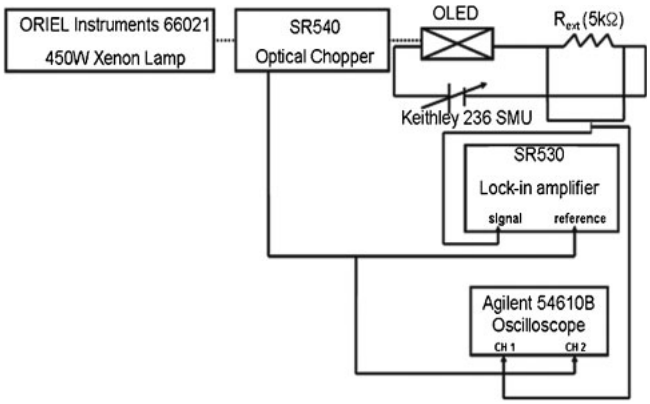

Fig. 1. Block diagram of the experimental setup used for the measurement of the modulated photocurrent. The device is irradiated by the light from a Xenon light source chopped by a rotating blade. The modulated photocurrent and the phase change were measured using a lock-in amplifier and oscilloscope.

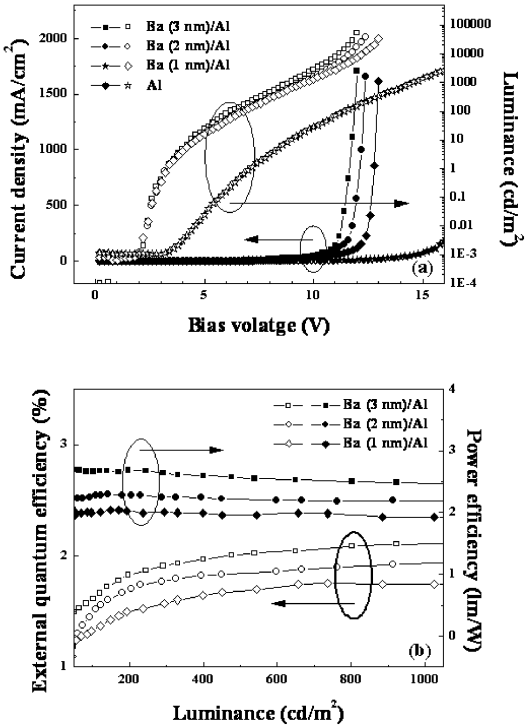

Fig. 2. (a) Current density and luminance curves as a function of applied bias voltage. (b) External quantum efficiency and power efficiency as a function of luminance. The devices were composed of glass/ITO/2-TNATA (30 nm)/NPB (18 nm)/Alq_3 (62 nm)/Ba (x nm)/Al (150 nm) (Ba thickness of devices 1, 2, 3, 4 = 3, 2, 1, 0 nm).

the bead, and curing the epoxy in a dry nitrogen box. The emissive active area of the devices was $2.0 \times 2.0\,mm^2$.

The device used for measuring the V_{BI} was fabricated as a glass/ITO (about 10 Ω/square, Geomatec Co., Ltd.)/Alq_3 (150 nm)/Ba (x nm, $x = 3$, 2, 1, and 0 nm)/Al (150 nm) structure. Figure 1 shows a block diagram of the experimental setup used to measure the modulated photocurrent. The OLED was connected in series with a 5 kΩ external resistance, and these two devices were electrically connected to a Keithley 236 source-measuring unit to apply a bias voltage, V_{Bias}. The device was irradiated by the light from a 450 W Xenon light source (ORIEL Instruments 66021) chopped by a rotating blade (Stanford Research SR540). The modulated frequency was set to 20 Hz. The modulated photocurrent generated in the diode was measured as a function of V_{Bias} using a lock-in amplifier (Stanford Research SR530) and oscilloscope (Agilent 54610B). The phase-sensitive lock-in amplifier was used to measure the magnitude and phase of the photocurrent.

The current density–voltage–luminance (J–V–L) characteristics were measured using a source-measure unit (Keithley 2400), while the emission intensities from the OLEDs devices were evaluated by measuring the photocurrent induced in a silicon photodiode (Oriel 71608) with a picoammeter (Keithley 485). The electroluminescence (EL) spectra of the as-fabricated devices were measured by optical emission spectroscopy (SC Tech. PCM-420).

3. Results and Discussion

To efficiently inject electrons, the introduction of Ba, with its low work function of 2.7 eV between the adjoining cathode layer (Al) and the Alq_3 layer, was expected to reduce the electron injection barrier by lowering the highest occupied molecular orbital (HOMO) level in the interface formed between Ba and Alq_3, as shown in ref. 7. Therefore, the use of Ba should improve the device performance by providing efficient electron injection.

Figure 2(a) shows the J–V–L characteristics of the four devices, 1–4. The J–V–L characteristics for the devices are also summarized in Table I. The turn-on voltages (V_T) at a luminance of about 0.1 cd/m^2 for devices 1, 2, 3, and 4 were 2.6, 2.8, 2.8, and 6.2 V, respectively. As shown in Fig. 2(a) and Table I, at a luminance of about 100 cd/m^2 (L_{100}), the current densities (J) of devices 1, 2, and 3 were 3.9 (6.2 V), 3.8 (6.6 V), and 3.9 mA/cm^2 (6.8 V), while their maximum luminances (L_{max}) were 54300 (12.0 V), 39400 (12.4 V), and 33300 cd/m^2 (12.8 V), respectively. Figure 2(b) shows the external quantum efficiencies (η_{ext}) and power efficiencies (η_{PE}) for devices 1–3 as a function of the luminance, and the results at L_{100} are summarized in Table I. As shown in Fig. 2(b) and Table I, the η_{PE} values at L_{100} for devices 1, 2, and 3 were 2.7, 2.2, and 2.0 lm/W and their η_{ext} values at L_{100} were 1.6, 1.5, and 1.3%, respectively. When the device characteristics such as V_T, J, L_{max}, η_{ext}, and η_{PE} were compared, device 1 with the cathode structure of Ba (3 nm)/Al (150 nm) showed the best light-emitting characteristics.

The maximum peak wavelengths (λ_{max}) of the EL spectra of the OLEDs with the Ba (x nm, $x = 3$, 2, 1, and 0 nm)/Al (150 nm) cathode were 532, 532, 532, and 534 for devices 1, 2, 3, and 4, respectively, as summarized in Table I. The EL characteristics of the devices used in this study were similar to each other.

Figure 3 shows a schematic diagram of the energy levels of a generic electrode/organic layer/electrode OLED, as a function of V_{Bias}. The change in the magnitude of the photocurrent can be understood by referring to the modulated photocurrent technique based on the following mechanism.[19] When the device is irradiated, the organic layer absorbs the incident light and the electrons are excited from a lower energy level to a higher one. If V_{Bias} is zero ($V_{Bias} < V_{BI}$), at thermodynamic equilibrium, the Fermi levels align to generate V_{BI} across the organic layer and the

Table I. *J–V–L* characteristics and EL properties of the devices composed of glass/ITO/2-TNATA (30 nm)/NPB (18 nm)/Alq_3 (62 nm)/Ba (x nm)/Al (150 nm) (Ba thickness of devices 1, 2, 3, 4 = 3, 2, 1, 0 nm).

Devices	Thickness of Ba (x nm) in Ba/Al	EL λ_{max} (nm) at 100 cd/m^2	η_{PE} (lm/W) at 100 cd/m^2	η_{ext} (%) at 100 cd/m^2	L_{max} (cd/m^2)	V (V) at 100 cd/m^2
1	3.0	534	2.7	1.6	54300 at 12 V	6.2 at 3.9 mA/cm^2
2	2.0	534	2.3	1.5	39400 at 12.4 V	6.6 at 3.8 mA/cm^2
3	1.0	534	2.0	1.3	33300 at 12.8 V	6.8 at 3.9 mA/cm^2
4	0	532	—	—	4400 at 18.2 V	—

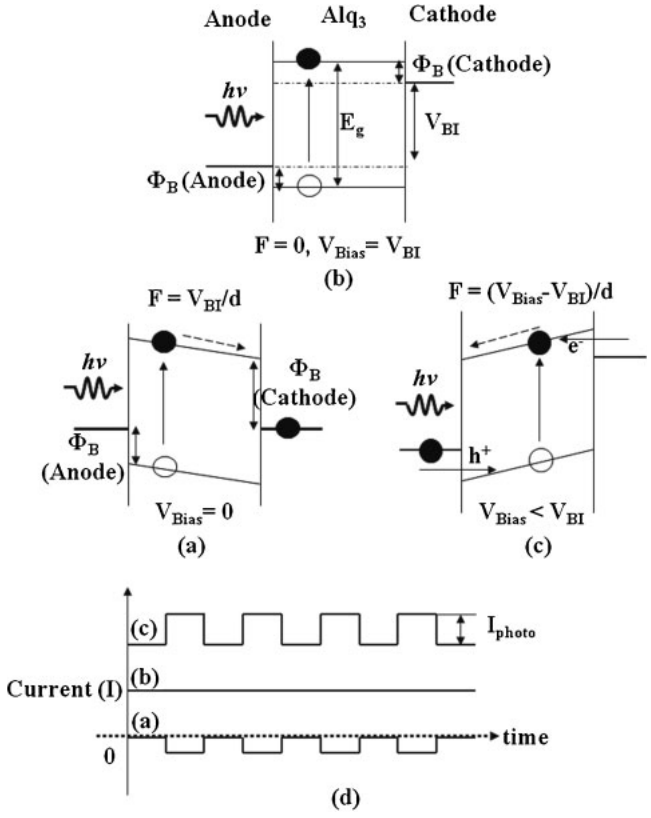

Fig. 3. (a) Schematic diagram of the energy levels of a generic electrode/organic layer/cathode as a function of the applied bias voltage [$V_{Bias} = 0$ (b), $V_{Bias} = V_{BI}$ (a), and $V_{Bias} > V_{BI}$ (c)] and the phase change of the photocurrent (d) as a function of the applied bias voltage. Here, E_g is the HOMO–LUMO gap of the organic layer.

excited electrons drift on the average built-in electric field, as shown in Fig. 3(a). Therefore, a photocurrent is generated even at zero bias voltage. In addition, V_{BI} is induced by the electron transfer from the electrode with the smaller work function (i.e., cathode) to the higher work-function anode. Without any significant charge (extrinsic or intrinsic) accumulation inside the organic layer, the electric field is essentially uniform in the bulk of the organic layer.

If V_{Bias} compensates for V_{BI}, flat band conditions are achieved, so that $V_{Bias} = V_{BI}$, as shown in Fig. 3(b). Here, the average electric field is zero and no photocurrent flows. At biases greater than V_{BI}, the field is $F = (V_{Bias} - V_{BI})/d > 0$, and this promotes the injection of carriers through the interfacial barriers [Fig. 3(c)]. The degree of injection will depend strongly on the magnitude of the field and the height of the barriers and, thus, on V_{BI}.[18)]

In a phase of the photocurrent, when V_{Bais} is greater than V_{BI}, an electric field is generated across the organic layer in the opposite direction [Fig. 3(c)] to that in the case where $V_{Bias} < V_{BI}$ [Fig. 3(a)]. In this situation, the photocurrent flows in the opposite direction [Fig. 3(a)], which causes the phase of the photocurrent to change by 180°, as shown in Fig. 3(d).

In designing the OLEDs with the Ba/Al cathode, the strategy we used herein was to build a series of devices differing only by the cathode contact material (by varying the Ba thickness), while keeping the organic layer and anode constant [E_g = constant, Φ_B (anode) constant], thereby establishing the linear dependence between V_{BI} and Φ_B at the modified cathode/organic layer [i.e., Φ_B (cathode)]. Figure 4(a) shows the magnitude and phase of the modulated photocurrent measured using a lock-in amplifier as a function of V_{Bias}. Figure 4(a) presents the result obtained from the ITO/Alq_3 (150 nm)/Ba (3 nm)/Al (150 nm) device and Fig. 4(b) shows V_{BI} and Φ_B for electron injection for devices 1–3. Figure 4(a) shows that as V_{Bias} increased, the magnitude of the photocurrent decreased up to a certain voltage, and then increased again. In this case, the voltage corresponding to the minimum photocurrent was V_{BI}. At around this voltage, the phase of the photocurrent changed by about 180°. In this way, V_{BI} values of 1.5, 1.5, 1.4, 1.3, and 0.4 were obtained at Ba thicknesses of 5.0, 3.0, 2.0, 1.0, 0.5, and 0 nm, respectively. The barrier height for electron injection (Φ_B^n) is represented by the following equation:[18,19,21)]

$$\Phi_B^n \text{ (eV)} = \Phi_{anode} \text{ (eV)} - E_{LUMO} \text{ (eV)} - V_{BI} \text{ (eV)}.$$

Here, Φ_{anode} and E_{LUMO} correspond to the work function of the anode (ITO: 4.7 eV)[25)] and the energy level of LUMO of Alq_3 (3.1 eV),[26)] respectively. The Φ_B^n values for devices 1, 2, 3, and 4 were 0.1, 0.2, 0.3, and 1.3 eV, respectively. Φ_B^n is strongly dependent on the work function of the Ba/Al cathode system used in this study. When compared to the *J–V–L* data of Fig. 2, increasing the Ba thickness from 0 to 3 nm improved the light-out coupling properties and, thus, reduced Φ_B^n by lowering the HOMO level of the interface formed between Ba/Al and Alq_3. As a result, it can be inferred that the device efficiency afforded by the balanced electron/hole population was improved by the increase in the number of electron carriers, because the structure of the organic layers and the anode remained the same.

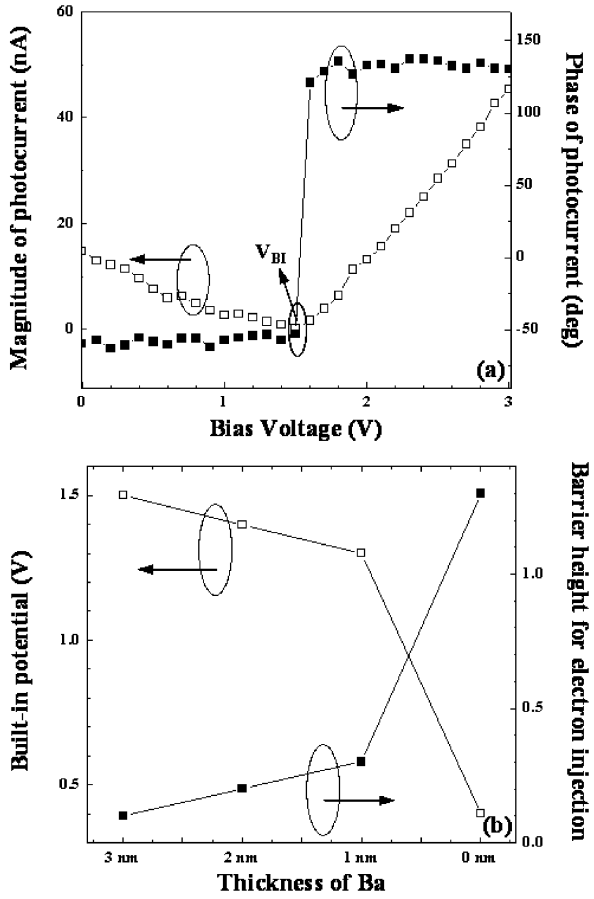

Fig. 4. (a) Magnitude and phase of the modulated photocurrent measured from device 1 with the structure (a) ITO/Alq_3 (150 nm)/Ba (3 nm)/Al (150 nm) and (b) built-in voltage as a function of the Ba layer thickness. The open and solid squares represent the built-in voltage and the barrier height for electron injection, respectively, in the ITO/Alq_3 (150 nm)/Ba (x nm, x = 3, 2, 1, and 0 nm)/Al (150 nm) device.

4. Conclusions

The device with the structure of glass/ITO/2-TNATA (30 nm)/NPB (18 nm)/Alq_3 (62 nm)/Ba (3 nm)/Al (150 nm) showed the highest light-emitting characteristics with an L_{max} of 54000 cd/m^2 and η_{PE} of 2.7 lm/W, as compared to the other devices with a Ba thickness of less than 3 nm. Also, in the device with the ITO/Alq_3 (150 nm)/Ba (x nm, x: 3, 2, 1, 0 nm)/Al (150 nm) structure, V_{BI} measured by using the modulated photocurrent technique had a higher value of 1.5 V, compared to those of the other devices with a Ba thickness of less than 3 nm. This study on the use of the modulated photocurrent technique demonstrated that the electron injection characteristics are strongly dependent on the thickness of the Ba layer in the cathode and that this technology can be easily applied to tune the work function of the interface of other cathode systems.

Acknowledgment

This research was supported by a grant (PAD-4) from Information Display R&D Center, one of the 21st Century Frontier R&D Program funded by the Ministry of Knowledge Economy of Korean government.

1) F. Gutmann and L. E. Lyons: *Organic Semiconductors* (Wiley, New York, 1997).
2) C. W. Tang and S. A. VanSlyke: Appl. Phys. Lett. **51** (1987) 913.
3) C. W. Tang: Appl. Phys. Lett. **48** (1986) 183.
4) L. Wang, D. Fine, D. Sharma, L. Torsi, and A. Dodabalapur: Anal. Bioanal. Chem. **384** (2006) 310.
5) H. Ishii, K. Sugiyama, E. Ito, and K. Seki: Adv. Mater. **11** (1999) 605.
6) J. Campbell: J. Vac. Sci. Technol. A **21** (2003) 521.
7) M. G. Mason, C. W. Tang, L.-S. Hung, P. Raychaudhuri, J. Madathil, D. J. Giesen, L. Yan, Q. T. Le, Y. Gao, S.-T. Lee, L. S. Liao, L. F. Cheng, W. R. Salaneck, D. A. dos Santos, and J. L. Brédas: J. Appl. Phys. **89** (2001) 2756.
8) X. Zhou, M. Pfeiffer, J. S. Huang, J. Biochwitz-Nimoth, D. S. Qin, A. Werner, J. Drechsel, B. Maennig, and K. Leo: Appl. Phys. Lett. **81** (2002) 922.
9) V. Choong, Y. Park, Y. Gao, T. Wehrmeister, K. Mullen, B. R. Heieh, and C. W. Tang: Appl. Phys. Lett. **69** (1996) 1492.
10) V.-E. Choong, Y. Park, Y. Gao, T. Wehrmeister, K. Mullen, B. R. Heieh, and C. W. Tang: J. Vac. Sci. Technol. A **15** (1997) 1745.
11) Y. Park, V.-E. Choong, B. R. Hsieh, C. W. Tang, and Y. Gao: Phys. Rev. Lett. **78** (1997) 3955.
12) M. Stoessel, G. Wittmann, J. Staudigel, F. Steuber, J. Blassong, W. Roth, H. Klausmann, W. Rogler, J. Simmerer, A. Winnacker, M. Inbasekaran, and E. P. Woo: J. Appl. Phys. **87** (2000) 4467.
13) J. Kido and T. Matsumoto: Appl. Phys. Lett. **73** (1998) 2866.
14) G. Parthasarathy, C. Shen, A. Kahn, and S. R. Forrest: J. Appl. Phys. **89** (2001) 4986.
15) L. S. Hung, C. W. Tang, and M. G. Mason: Appl. Phys. Lett. **70** (1997) 152.
16) T. Mori, H. Fujikawa, S. Tokito, and Y. Taga: Appl. Phys. Lett. **73** (1998) 2763.
17) F. Li, H. Tang, J. Anderegg, and S. Shinar: Appl. Phys. Lett. **70** (1997) 1233.
18) T. M. Brown, J. S. Kim, R. H. Friend, F. Cacialli, R. Daik, and W. J. Feast: Appl. Phys. Lett. **75** (1999) 1679.
19) T. M. Brown, R. H. Friend, I. S. Millard, D. J. Lacey, T. Butler, J. H. Burroughes, and F. Cacialli: J. Appl. Phys. **93** (2003) 6159.
20) D. Ray, M. P. Patankar, N. Periasamy, and K. L. Narasimhan: Synth. Met. **155** (2005) 349.
21) J. T. Lim, J. H. Lee, G. Y. Yeom, E. H. Lee, and T. W. Kim: J. Vac. Sci. Technol. A **26** (2008) 961.
22) W. Benenson, J. W. Harris, H. Stocker, and H. Luttz: *Handbook of Physics* (AIP Press, New York, 2002).
23) X. Zeng, M. Tavasli, I. F. Perepichka, A. S. Batsanov, M. R. Bryce, C.-J. Chiang, C. Rothe, and A. P. Monkman: Chem.—Eur. J. **14** (2008) 933.
24) E. Wang, C. Li, J. Peng, and Y. Cao: J. Polym. Sci., Part A **45** (2007) 4941.
25) G. Partharathy, P. E. Burrows, V. Khalfin, V. G. Kozlov, and S. R. Forrest: Appl. Phys. Lett. **72** (1998) 2138.
26) M. A. Baldo and S. R. Forrest: Phys. Rev. B **62** (2000) 10958.